Ab–initio calculation of Kerr spectra for semi–infinite systems including multiple reflections and optical interferences

A. Vernes

Center for Computational Materials Science,

Technical University Vienna, Gumpendorferstr. 1a, A–1060 Vienna, Austria

L. Szunyogh

Center for Computational Materials Science,

Technical University Vienna, Gumpendorferstr. 1a, A–1060 Vienna, Austria

Department of Theoretical Physics, Budapest University of Technology and Economics,

Budafoki út 8, H–1521 Budapest, Hungary

P. Weinberger

Center for Computational Materials Science,

Technical University Vienna, Gumpendorferstr. 1a, A–1060 Vienna, Austria

(November 27, 2001)

Abstract

Based on Luttinger's formulation the complex optical conductivity tensor is calculated within the framework of the spin–polarized relativistic screened Korringa–Kohn–Rostoker method for layered systems by means of a contour integration technique. For polar geometry and normal incidence ab–initio Kerr spectra of multilayer systems are then obtained by including via a 2×2 matrix technique all multiple reflections between layers and optical interferences in the layers. Applications to Co|Pt_5 and Pt_3 |Co|Pt_5 on the top of a semi–infinite fcc–Pt(111) bulk substrate show good qualitative agreement with the experimental spectra, but differ from those obtained by applying the commonly used

two–media approach.

PACS numbers: 71.15.Rf, 75.50.Ss, 78.20.Ls, 78.66.Bz

I. INTRODUCTION

Magneto-optical effects not only provide a powerful tool in probing the magnetic properties of solids, [1–3] but are also of direct technological interest as phenomena to be used for high–density magneto–optical recording. [2,4] Up to now, however, realistic theoretical investigations were lacking, because band–structure methods using supercells, [5] cannot provide an adequate description of layered systems, for which special computational techniques such as the spin–polarized relativistic screened Korringa–Kohn–Rostoker (SKKR) method have been designed. [6–8] Furthermore, the absorptive parts of the optical conductivity tensor as obtained from the inter–band contributions, [9] are not sufficient for magneto–optical Kerr spectra calculations, since also the dissipative parts have to be known. Hence, in supercell type calculations, besides the necessity to use the Kramers–Kronig relations, one has to include also the inter–band contributions by means of a semi–empirical Drude term. [10] Only recently a better scheme was developed by two of the present authors [11], in which a contour integration is used to obtain the complex optical conductivity tensor as based Luttinger's formula, [12] which in turn includes all inter– and intra–band contributions. [13] Combining this contour integration technique with the SKKR method, realistic inter– and intra–layer complex optical conductivities can be obtained for layered systems.

Having evaluated the inter– and intra–layer optical conductivities, the magneto–optical Kerr spectra can then be calculated by using a macroscopical model such as, e.g., the two–media approach. [14] Because the layered system contains more boundaries than just the interface between the vacuum and the surface layer, the two–media approach not fully includes the dynamics of the electromagnetic waves propagation in such systems. Since the pioneering work of Abelés in 1950, [15] several methods are known in the literature [16,17] to treat multiple reflections and interferences using either a 2×2 matrix [18,19] or 4×4 matrix [20–22] technique. In the present paper the magneto–optical Kerr spectra of layered systems are evaluated for the most frequently used experimental set–up, namely polar geometry and normal incidence, by making use of the complex optical conductivity tensor and the 2×2 matrix technique.

In Section II the theoretical background is reviewed briefly. Computational aspects are then summarized in Section III. In Section IV the two–media approach (Sect. IV A) and the applied

2×2 matrix technique (Sect. IV C) are viewed as two different macroscopic models of how to calculate magneto–optical Kerr spectra of layered systems. Particular emphasis has been put in Sect. IV B on the construction of layer–resolved permittivities in terms of the (macroscopic) material equation within linear response. This construction method combined with the 2×2 matrix technique, allows one to determine self–consistently layer–resolved permittivities, see Sect. IV C 4. As an illustration ab–initio Kerr spectra of Co|Pt multilayer systems are presented and discussed in Section V. Finally, in Section VI the main results are summarized.

II. THEORETICAL FRAMEWORK

A. Luttinger's formalism

The frequency dependent complex optical conductivity tensor $\tilde{\boldsymbol{\sigma}}(\omega)$ can be evaluated starting from the well–known Kubo formula and using a scalar potential description of the electric field. [23] However, by using the equivalent [24] vector potential description of the electric field, one ends up with Luttinger's formula: [12]

$$\tilde{\sigma}_{\mu\nu}(\omega) = \frac{\tilde{\Sigma}_{\mu\nu}(\omega) - \tilde{\Sigma}_{\mu\nu}(0)}{\hbar\omega + i\delta} \ , \tag{1}$$

with the current–current correlation function as given by [25]

$$\tilde{\Sigma}_{\mu\nu}(\omega) = \frac{i\hbar}{V} \sum_{m,n} \frac{f(\epsilon_n) - f(\epsilon_m)}{\hbar\omega + i\delta + (\epsilon_n - \epsilon_m)} J^{\mu}_{nm} J^{\nu}_{mn} \ . \tag{2}$$

Here $f(\epsilon)$ is the Fermi–Dirac distribution function, ϵ_m, ϵ_n a pair of eigenvalues of the one–electron Hamiltonian, the J^{μ}_{mn} are matrix elements of the electronic current operator ($\mu = \mathrm{x}, \mathrm{y}, \mathrm{z}$) and V the reference (crystalline) volume.

The positive infinitesimal δ implies the electromagnetic field to be turned on at $t = -\infty$ and hence describes the interaction of the system with its surrounding. [26] However, as can be seen from Eq. (2), δ can be also viewed as a finite life–time broadening, which accounts for all scattering processes at a finite temperature.

Luttinger's formula (1) and Eq. (2) have several advantages over the commonly used optical conductivity tensor formula of Callaway. [9] First of all, in contrast to the latter, Eq. (1)

simultaneously provides both, the absorptive and the dissipative parts of the optical conductivity tensor. Hence there is no need for using the Kramers–Kronig relations in the Luttinger's formalism. On the other hand, as recently was shown [13] Luttinger's formalism accounts for both, the inter– and the intra–band contribution on the same footing. Thus by using Eq. (1) in combination with Eq. (2), one does not need to include a phenomenological Drude term in order to simulate the intra–band contribution. [5] Furthermore, as was also demonstrated [13] Eqs. (1) and (2) can be used for calculations in the static ($\omega = 0$) limit, provided the life–time broadening is kept finite ($\delta \neq 0$).

B. Contour integration technique

Instead of evaluating the sums in the expression for the current–current correlation function (2) over eigenvalues of the one–electron Hamiltonian, $\tilde{\Sigma}_{\mu\nu}(\omega)$ can be calculated by means of a contour integration in the complex energy plane.

For the selection of a particular contour Γ, this technique [11] exploits the facts that with the exception of the Matsubara poles $z_k = \varepsilon_{\rm F} + i\,(2k-1)\,\delta_T$ ($k = 0, \pm 1, \pm 2, \ldots$, and $\delta_T = \pi k_{\rm B} T$), [27] in both semi–planes the Fermi–Dirac distribution function of complex argument $f(z)$ is analytical [25] and is a real function for complex energies $z = \varepsilon \pm i\delta_j$ situated in–between two successive Matsubara poles. [28] The latter property of $f(z)$, e.g., is exploited by using $\delta_j = 2N_j\delta_T$, where N_1 is the number of Matsubara poles included in Γ in the upper semi–plane and N_2 in the lower semi–plane. [11]

By applying the residue theorem, it has been shown [11] that equivalently to Eq. (2) one has

$$\tilde{\Sigma}_{\mu\nu}(\omega) = \oint\!\!\!\!\!\!\circlearrowright_{\Gamma} dz\; f(z)\; \tilde{\Sigma}_{\mu\nu}(z+\zeta, z) - \left[\oint\!\!\!\!\!\!\circlearrowright_{\Gamma} dz\; f(z)\; \tilde{\Sigma}_{\mu\nu}(z-\zeta^*, z)\right]^* - 2i\delta_T \sum_{k=-N_2+1}^{N_1} \left[\tilde{\Sigma}_{\mu\nu}(z_k+\zeta, z_k) + \tilde{\Sigma}^*_{\mu\nu}(z_k-\zeta^*, z_k)\right] \;, \tag{3}$$

such that

$$\tilde{\Sigma}_{\mu\nu}(0) = \oint\!\!\!\!\!\!\circlearrowright_{\Gamma} dz\; f(z)\; \tilde{\Sigma}_{\mu\nu}(z, z) - 2i\delta_T \sum_{k=-N_2+1}^{N_1} \tilde{\Sigma}_{\mu\nu}(z_k, z_k) \;, \tag{4}$$

where $\zeta = \hbar\omega + i\delta$ and the kernel

$$\tilde{\Sigma}_{\mu\nu}(z_1, z_2) = -\frac{\hbar}{2\pi V}\ \mathrm{Tr}\ \left[J^{\mu}\ G(z_1)\ J^{\nu}\ G(z_2)\right]\ , \tag{5}$$

is related to the electronic Green function $G(z)$. The auxiliary quantity $\tilde{\Sigma}_{\mu\nu}(z_1, z_2)$ has already been used in residual resistivity calculations ($\omega, T = 0$) of substitutionally disordered bulk systems [29] and magneto–transport calculations of inhomogeneously disordered layered systems. [30] Only recently, however, it has been shown, [13] that Eqs. (3)–(5) preserve all the advantages and features of Luttinger's formalism as was mentioned already above.

In the present paper, $\tilde{\Sigma}_{\mu\nu}(z_1, z_2)$ is evaluated in terms of relativistic current operators [30] and the Green functions provided by the spin–polarized relativistic SKKR method for layered systems [6–8]. The optical conductivity tensor of a multilayer system is then given [31] by

$$\tilde{\boldsymbol{\sigma}}(\omega) = \sum_{p=1}^{N}\sum_{q=1}^{N}\tilde{\boldsymbol{\sigma}}^{pq}(\omega)\ , \tag{6}$$

with $\tilde{\boldsymbol{\sigma}}^{pq}(\omega)$ refering to either the inter– ($p \neq q$) or the intra–layer ($p = q$) contribution to the optical conductivity tensor.

III. COMPUTATIONAL DETAILS

In addition to the number of Matsubara poles considered, the optical conductivity tensor depends also on the number of complex energy points n_z used in order to evaluate the energy integrals in Eqs. (3) and (4), on the number of $\vec{k}$ –points used to calculate the scattering path operators that define the Green functions [7] and $\tilde{\Sigma}_{\mu\nu}(z \pm \hbar\omega + i\delta, z)$ for a given energy z. Recently, the present authors have proposed two schemes to control the accuracy of these z– and $\vec{k}$–integrations. [32]

The first of these schemes is meant to control the accuracy of the z–integrations along each contour part by comparing the results obtained from the Konrod quadrature [33,34], $\mathcal{K}_{2n_z+1}\tilde{\Sigma}_{\mu\nu}(\omega)$, with those from the Gauss integration rule, $\mathcal{G}_{n_z}\tilde{\Sigma}_{\mu\nu}(\omega)$. [35] On a particular part of the contour $\tilde{\Sigma}_{\mu\nu}(\omega)$ is said to be converged, if the following convergence criterion: [32]

$$\max\ \left|\ \mathcal{K}_{2n_z+1}\tilde{\Sigma}_{\mu\nu}(\omega) - \mathcal{G}_{n_z}\tilde{\Sigma}_{\mu\nu}(\omega)\ \right| \leq \varepsilon_z\,, \tag{7}$$

is fulfilled for a given accuracy parameter ε_z.

The other scheme refers to the cumulative special points method, [32] which permits to perform two–dimensional $\vec{k}$ –space integrations with arbitrary high precision. This method exploits the arbitrariness of the special points mesh origin. [36] For a given (arbitrary high) accuracy $\epsilon_{\vec{k}}$ the following convergence criterion has to apply

$$\max \left| \mathcal{S}_{n_i} \tilde{\Sigma}_{\mu\nu}(z', z) - \mathcal{S}_{n_{i-1}} \tilde{\Sigma}_{\mu\nu}(z', z) \right| \leq \varepsilon_{\vec{k}} \,, \tag{8}$$

for any complex energy z on the contour or z_k Matsubara pole. Here $n_i = 2^{i+2} n_0$ ($n_0 \in N$) is the number of divisions along each primitive translation vector in the two–dimensional $\vec{k}$–space and $z' = z + \zeta$, $z - \zeta^*$.

In the present paper, the optical conductivity tensor calculations were carried out for $T =$ 300 K, using a life–time broadening of 0.048 Ryd and $N_2 = 2$ Matsubara poles in the lower semi–plane. Because the computation of $\tilde{\sigma}_{\mu\nu}(\omega)$ does not depend on the form of the contour, [32] in the upper semi–plane we have accelerated the calculations by considering $N_1 = 37$ Matsubara poles. The convergence criteria (7) and (8) were fulfilled for $\varepsilon_z = \varepsilon_{\vec{k}} = 10^{-3}$ a.u. .

IV. MAGNETO–OPTICAL KERR EFFECT

In the case of the polar magneto–optical Kerr effect (PMOKE), [14] the Kerr rotation angle

$$\theta_{\rm K} = -\frac{1}{2} \left(\Delta_+ - \Delta_- \right) \tag{9}$$

and the Kerr ellipticity

$$\varepsilon_{\rm K} = -\frac{r_+ - r_-}{r_+ + r_-} \tag{10}$$

are given in terms of the complex reflectivity of the right– (+) and left–handed (–) circularly polarized light

$$\tilde{r}_\pm = \frac{\mathcal{E}_\pm^{(\rm r)}}{\mathcal{E}^{(\rm i)}} = r_\pm \, e^{i\Delta_\pm} \,. \tag{11}$$

Here the complex amplitude of the reflected right– and left–handed circularly polarized light is denoted by $\mathcal{E}_\pm^{(\rm r)}$ and that of the incident light by $\mathcal{E}^{(\rm i)}$; $\Delta_\pm$ is the phase of the complex

reflectivity $\tilde{r}_{\pm}$ and $r_{\pm} = |\tilde{r}_{\pm}|$. Eqs. (9) and (10) are exact, which can be easily deduced from simple geometrical arguments. However, in order to apply these relations, one needs to make use of a macroscopic model for the occurring reflectivities.

A. Macroscopic model I: the two–media approach

This simplest and most commonly used macroscopic model treats the multilayer system as a homogeneous, anisotropic, semi–infinite medium, such that the incident light is reflected only at the boundary between the vacuum and the surface (top) layer.

In case of normal incidence the two–media approach provides an appropriate formula for the complex Kerr angle [14]

$$\tilde{\Phi}_{\mathrm{K}} \equiv \theta_{\mathrm{K}} - i\varepsilon_{\mathrm{K}} = i\frac{\tilde{r}_{+} - \tilde{r}_{-}}{\tilde{r}_{+} + \tilde{r}_{-}} \ , \tag{12}$$

which can be deduced from Eqs. (9) and (10) by assuming a small difference in the complex reflectivity of the right– and left–handed circularly polarized light. Because Im $\tilde{\sigma}_{\mathrm{xy}}(\omega)$ usually is almost a hundred times smaller than Re $\tilde{\sigma}_{\mathrm{xx}}(\omega)$, see Ref. [13], the average complex refractive index of the right– and left–handed circularly polarized light is dominated by $\tilde{\sigma}_{\mathrm{xx}}(\omega)$ and hence the following direct formula results from Eq. (12): [14]

$$\tilde{\Phi}_{\mathrm{K}} \approx \frac{\tilde{\sigma}_{\mathrm{xy}}(\omega)}{\tilde{\sigma}_{\mathrm{xx}}(\omega)} \frac{1}{\sqrt{1 - \dfrac{4\pi i}{\omega}\tilde{\sigma}_{\mathrm{xx}}(\omega)}} \ , \tag{13}$$

with $\tilde{\boldsymbol{\sigma}}(\omega)$ as given by Eq. (6). It should be noted that the "direct" formula in Eq. (13) was introduced by Reim and Schoenes [14] in order to extract the optical conductivity tensor elements $\tilde{\sigma}_{\mathrm{xx}}(\omega)$ and $\tilde{\sigma}_{\mathrm{xy}}(\omega)$ from experimental PMOKE data.

B. Macroscopic model II: layer–resolved permittivities

Within linear response theory [37] the Fourier transformed macroscopic material equations, [38] averaged over the reference volume V, directly yields the total electric displacement

$$\frac{1}{V}\int_{V} d^3r \ \vec{D}(\vec{r},\omega) = \frac{1}{V}\int_{V} d^3r \int_{V} d^3r' \ \tilde{\boldsymbol{\epsilon}}(\omega;\vec{r},\vec{r}')\,\vec{E}(\vec{r}',\omega) \ , \tag{14}$$

provided that the dielectric function $\tilde{\boldsymbol{\epsilon}}\left(\omega;\vec{r},\vec{r}'\right)$ and the Fourier components of the electric field $\vec{E}\left(\vec{r}',\omega\right)$ are known.

Using non–overlapping cells in configuration space (Atomic Sphere Approximation (ASA), applied in the present approach), the reference volume can be written as

$$V = \sum_{p=1}^{N}\left(N_{\parallel}\sum_{i}\Omega_{pi}\right) \equiv \sum_{p=1}^{N}\Omega^{p} \ ,$$

where $N_{\parallel}$ is the number of atoms per layer (the same 2D lattice has to apply for each layer p), N the total number of layers and Ω_{pi} the volume of the ith atomic sphere in layer p.

Assuming that plane waves propagate in a layer like in a two–dimensional unbound homogeneous medium and that $\vec{D}_{pi}\left(\vec{r},\omega\right) = \vec{D}_{p}\left(\vec{r},\omega\right)$, the integral on the left hand side of Eq. (14) can be written within the ASA as

$$\int_{V} d^{3}r \ \vec{D}\left(\vec{r},\omega\right) = N_{\parallel}\sum_{p=1}^{N}\vec{\mathcal{D}}_{p}\sum_{i}\Omega_{pi}\left[1+6\sum_{k=1}^{\infty}\frac{\left(-1\right)^{k}\left(k+1\right)}{\left(2k+3\right)!}\left(\frac{2\pi}{\lambda_{0}}n_{p}S_{pi}\right)^{2k}\right] \ , \qquad (15)$$

where $\vec{\mathcal{D}}_{p}$ is the amplitude of the electric displacement, $\vec{n}_{p}$ is the refraction vector,

$$\vec{n}_{p} = \frac{\vec{q}_{p}}{q_{0}} \ , \qquad (16)$$

$\vec{q}_{p}$ the wave vector ($q_{0} = 2\pi/\lambda_{0}$ refers to the propagation constant in vacuum) and S_{pi} is the radius of the ith atomic sphere in layer p. Accordingly, the double integral on the right hand side of Eq. (14) reduces to

$$\begin{aligned}\int_{V} d^{3}r \int_{V} d^{3}r' \ \tilde{\boldsymbol{\epsilon}}\left(\omega;\vec{r},\vec{r}'\right)\vec{E}\left(\vec{r}',\omega\right) \ = \left(4\pi\right)^{2} N_{\parallel}\sum_{p,q=1}^{N}\vec{\mathcal{E}}_{q}\sum_{i,j}\int_{0}^{S_{pi}} dr \ r^{2}\int_{0}^{S_{qj}} dr' \ \left(r'\right)^{2} \\ \tilde{\boldsymbol{\epsilon}}^{pi,qj}\left(\omega;r,r'\right) \ \left[1+\sum_{k=1}^{\infty}\frac{\left(-1\right)^{k}}{\left(2k+1\right)!}\left(\frac{2\pi}{\lambda_{0}}n_{q}r'\right)^{2k}\right] \ , \qquad (17)\end{aligned}$$

where $\vec{\mathcal{E}}_{q}$ is the amplitude of the electric field in layer q and $\tilde{\boldsymbol{\epsilon}}^{pi,qj}\left(\omega;r,r'\right)$ is the dielectric function $\tilde{\boldsymbol{\epsilon}}\left(\omega;\vec{r},\vec{r}'\right)$ at $\vec{r}\in\Omega_{pi}$ and $\vec{r}'\in\Omega_{qj}$.

In the case of visible light the wave vector dependence of the permittivity is negligeable. [14] Therefore, after having substituted Eqs. (15) and (17) into Eq. (14), only the first term in the power series expansions has to be kept, which immediately leads to

$$\sum_{p=1}^{N}\left[\vec{\mathcal{D}}_{p} - \sum_{q=1}^{N}\tilde{\boldsymbol{\epsilon}}^{pq}\left(\omega\right)\vec{\mathcal{E}}_{q}\right]\sum_{i}\Omega_{pi} = 0 \ ,$$

where the inter– ($p \neq q$), intra–layer ($p = q$) permittivities are given by

$$\tilde{\boldsymbol{\epsilon}}^{pq}(\omega) = \frac{(4\pi)^2}{\sum_i \Omega_{pi}} \sum_{i,j} \int_0^{S_{pi}} dr\ r^2 \int_0^{S_{qj}} dr'\ (r')^2\ \tilde{\boldsymbol{\epsilon}}^{pi,qj}(\omega; r, r')\ .$$

It should be noted that a similar result connecting the static current in layer p to the electric field in layer q is already known from electric transport theory in inhomogeneous [39] or layered systems [30]. By using the relation $\vec{\mathcal{D}}_p = \tilde{\boldsymbol{\epsilon}}^p(\omega)\, \vec{\mathcal{E}}_p$, the layer–resolved permittivities $\tilde{\boldsymbol{\epsilon}}^p(\omega)$ are then solutions of the following system of equations:

$$\tilde{\boldsymbol{\epsilon}}^p(\omega)\, \vec{\mathcal{E}}_p = \sum_{q=1}^{N} \tilde{\boldsymbol{\epsilon}}^{pq}(\omega)\ \vec{\mathcal{E}}_q\ , \qquad p = 1, \ldots, N\ . \tag{18}$$

By mapping the inter– and intra–layer contributions $\tilde{\boldsymbol{\sigma}}^{pq}(\omega)$ to the microscopically exact optical conductivity tensor $\tilde{\boldsymbol{\sigma}}(\omega)$, Eq. (6), onto the corresponding contributions of the permittivity tensor

$$\tilde{\boldsymbol{\epsilon}}^{pq}(\omega) = \frac{1}{N}\left[1 - \frac{4\pi i}{\omega}\tilde{\boldsymbol{\sigma}}^{pq}(\omega)\right]\ , \tag{19}$$

one then can establish a well–defined macroscopical model for the evaluation of Kerr spectra.

C. The 2×2 matrix technique

1. Multiple reflections and optical interferences

In contrast to the two–media approach the inclusion of all optical reflections and interferences within a multilayer system assumes that each layer acts as a homogeneous, anisotropic medium between two boundaries and is characterized by a layer–resolved dielectric tensor $\tilde{\boldsymbol{\epsilon}}^p$ ($p = 1, \ldots, N$). [18,19]

As a first step the Fresnel or characteristic equation: [40]

$$\left| n_p^2 \delta_{\mu\nu} - n_{p\mu} n_{p\nu} - \tilde{\epsilon}^p_{\mu\nu} \right| = 0 \qquad (\mu, \nu = \mathrm{x}, \mathrm{y}, \mathrm{z}) \tag{20}$$

has to be solved in order to determine the normal modes of the electromagnetic waves in a particular layer p. [41] Then by solving the Helmholtz equation for each normal modes, [41]

$$\sum_{\nu} \left(n_p^2 \delta_{\mu\nu} - n_{p\mu} n_{p\nu} - \tilde{\epsilon}^p_{\mu\nu} \right) \mathcal{E}_{p\nu} = 0 \qquad (\mu, \nu = \mathrm{x}, \mathrm{y}, \mathrm{z})\ , \tag{21}$$

the corresponding $\mathcal{E}_{p\nu}$ components of the electric field in layer p are deduced. After having obtained the $\mathcal{E}_{p\nu}$s , the curl Maxwell equation [18,19]

$$\vec{\mathcal{H}}_p = \vec{n}_p \times \vec{\mathcal{E}}_p \ , \tag{22}$$

provides the amplitudes of the magnetic fields $\vec{\mathcal{H}}_p$ for each normal mode in layer p. Here the Gaussian system of units has been used, $\vec{n}_p$ is the refraction vector, as given by Eq. (16), $\mid \vec{n}_p \mid = \tilde{n}_p$, which in an anisotropic medium is direction and frequency dependent. [40]

Finally, continuity of the tangential components of the electric and the magnetic field at the boundary between adjacent layers leads to a set of equations, which has to be solved recursively in order to determine the magneto–optical coefficients of the layered system, such as, e.g., the surface reflectivity. If no symmetry reduced quantities $\tilde{\boldsymbol{\epsilon}}^p$ are used all the previous steps, Eqs. (20)–(22), have to be performed numerically by using – for example – the 2×2 matrix technique of Mansuripur. [18,19]

Most frequently MOKE experiments are performed in polar geometry using normal incidence. Therefore in the following the 2×2 matrix technique of Mansuripur is confined to this particular experimental geometry. This reduction has the advantage that with the exception of the last step in which the surface reflectivity has to be evaluated, all the other steps can be carried out analytically.

In the case of cubic, hexagonal or tetragonal systems and the orientation of the magnetization $\vec{M}_p$ pointing along the surface normal (z–direction), the layer–resolved permittivity tensor is given by

$$\tilde{\boldsymbol{\epsilon}}^p = \begin{pmatrix} \tilde{\epsilon}^p_{\rm xx} & \tilde{\epsilon}^p_{\rm xy} & 0 \\ -\tilde{\epsilon}^p_{\rm xy} & \tilde{\epsilon}^p_{\rm xx} & 0 \\ 0 & 0 & \tilde{\epsilon}^p_{\rm zz} \end{pmatrix} \ . \tag{23}$$

Assuming that $\tilde{\epsilon}^p_{\rm zz} \simeq \tilde{\epsilon}^p_{\rm xx}$ $(p = 1, \ldots, N)$, the error introduced by this simplification – as easily can be shown – is proportional to the difference $\tilde{\epsilon}^p_{\rm zz} - \tilde{\epsilon}^p_{\rm xx}$, which in turn is usually small enough to be neglected. If in polar geometry the incidence is normal,

$$\tilde{n}_{p\rm x} = \tilde{n}_{p\rm y} = 0 \quad \text{for} \quad p = 1, \ldots, N \ ,$$

the characteristic equation (20) provides four normal modes of electromagnetic waves in a layer p:

$$\tilde{n}_{pz} = \pm\sqrt{\tilde{\epsilon}^p_{\rm xx} \pm i\tilde{\epsilon}^p_{\rm xy}} \ .$$

Two of these four solutions are always situated in the lower half and the other two in the upper half of the complex plane. The first two solutions, $\tilde{n}^{(1)}_{pz}$ and $\tilde{n}^{(2)}_{pz}$, correspond to a "downward" (negative z –direction) and the other two, $\tilde{n}^{(3)}_{pz}$ and $\tilde{n}^{(4)}_{pz}$, an "upward" (positive z–direction) propagation of the electromagnetic waves. [18,19] These two different kinds of cases are given by

$$\begin{cases} \tilde{n}^{(1)}_{pz} &= -\sqrt{\tilde{\epsilon}^p_{\rm xx} + i\tilde{\epsilon}^p_{\rm xy}} \\ \tilde{n}^{(2)}_{pz} &= -\sqrt{\tilde{\epsilon}^p_{\rm xx} - i\tilde{\epsilon}^p_{\rm xy}} \end{cases} \tag{24}$$

and

$$\begin{cases} \tilde{n}^{(3)}_{pz} &= \sqrt{\tilde{\epsilon}^p_{\rm xx} + i\tilde{\epsilon}^p_{\rm xy}} \\ \tilde{n}^{(4)}_{pz} &= \sqrt{\tilde{\epsilon}^p_{\rm xx} - i\tilde{\epsilon}^p_{\rm xy}} \end{cases} \ . \tag{25}$$

If in a given multilayer system a particular layer p is paramagnetic, its permittivity tensor $\tilde{\boldsymbol{\epsilon}}^p$ is again of form shown in Eq. (23), with $\tilde{\epsilon}^p_{\rm xy} = 0$ and $\tilde{\epsilon}^p_{\rm zz} = \tilde{\epsilon}^p_{\rm xx}$. In this case only two beams are propagating, namely those characterized by $\tilde{n}^{(1)}_{pz} \equiv \tilde{n}^{(2)}_{pz} = -\sqrt{\tilde{\epsilon}^p_{\rm xx}}$ and $\tilde{n}^{(3)}_{pz} \equiv \tilde{n}^{(4)}_{pz} = \sqrt{\tilde{\epsilon}^p_{\rm xx}}$. Furthermore, since the vacuum is a homogeneous, isotropic, semi–infinite medium, in addition to $\tilde{\epsilon}_{\rm xy} = 0$, $\tilde{\epsilon}_{\rm xx} = \tilde{\epsilon}_{\rm zz} = 1$.

For each solution $n^{(k)}_{pz}$ $(k = 1, \ldots, 4)$ of the characteristic equation (20), the electric field must satisfy the Helmholtz equation (21). Because not all of the equations are independent, these can be solved only for two components of the electric field keeping the third one arbitrary. Therefore, following the strategy proposed by Mansuripur, for beam 1 ($n^{(1)}_{pz}$) and beam 3 ($n^{(3)}_{pz}$), the corresponding $\mathcal{E}^{(k)}_{p\rm x}$ are chosen arbitrary, whereas for beam 2 ($n^{(2)}_{pz}$) and beam 4 ($n^{(4)}_{pz}$), the $\mathcal{E}^{(k)}_{p\rm y}$ are arbitrary. [18,19] For polar geometry and normal incidence, the solutions of the Helmholtz equation (21) are given in Table I and the corresponding components of the magnetic field as obtained from Eq. (22) are listed in Table II.

2. Layer–resolved reflectivity matrix

Numbering the layers starting from the first one on top of the substrate towards the surface, the surface layer has the layer index $p = N$, see Fig. 1. The 2×2 reflectivity matrix $\mathcal{R}_p$ at the lower boundary z_p of layer p is given by: [18,19]

$$\begin{pmatrix} \mathcal{E}_{p\mathrm{x}}^{(3)} \\ \mathcal{E}_{p\mathrm{y}}^{(4)} \end{pmatrix} = \mathcal{R}_p \begin{pmatrix} \mathcal{E}_{p\mathrm{x}}^{(1)} \\ \mathcal{E}_{p\mathrm{y}}^{(2)} \end{pmatrix} = \begin{pmatrix} \tilde{r}_p & 0 \\ 0 & \tilde{r}'_p \end{pmatrix} \begin{pmatrix} \mathcal{E}_{p\mathrm{x}}^{(1)} \\ \mathcal{E}_{p\mathrm{y}}^{(2)} \end{pmatrix} , \tag{26}$$

see also the explicit discussion in the Appendix. The tangential components of the electric and magnetic field at a point z_p^+ just above the boundary z_p are then given by

$$\begin{cases} \begin{pmatrix} \mathcal{E}_{p\mathrm{x}} \\ \mathcal{E}_{p\mathrm{y}} \end{pmatrix}_{z_p^+} = \mathcal{A}\,(\mathcal{I} + \mathcal{R}_p) \begin{pmatrix} \mathcal{E}_{p\mathrm{x}}^{(1)} \\ \mathcal{E}_{p\mathrm{y}}^{(2)} \end{pmatrix} \\ \begin{pmatrix} \mathcal{H}_{p\mathrm{x}} \\ \mathcal{H}_{p\mathrm{y}} \end{pmatrix}_{z_p^+} = \mathcal{B}_p^{12}\,(\mathcal{I} - \mathcal{R}_p) \begin{pmatrix} \mathcal{E}_{p\mathrm{x}}^{(1)} \\ \mathcal{E}_{p\mathrm{y}}^{(2)} \end{pmatrix} \end{cases} , \tag{27}$$

where according to Tables I and II,

$$\mathcal{A} \equiv \begin{pmatrix} 1 & i \\ i & 1 \end{pmatrix} , \qquad \mathcal{B}_p^{12} = \begin{pmatrix} -i\tilde{n}_{pz}^{(1)} & -\tilde{n}_{pz}^{(2)} \\ \tilde{n}_{pz}^{(1)} & i\tilde{n}_{pz}^{(2)} \end{pmatrix} \tag{28}$$

and $\mathcal{I}$ is the 2×2 unit matrix.

Using the lower boundary z_{p-1} as reference plane for the four beams in layer $p-1$, the tangential components of the electric and magnetic field at a point z_p^- just below the boundary z_p are of the form

$$\begin{cases} \begin{pmatrix} \mathcal{E}_{p\mathrm{x}} \\ \mathcal{E}_{p\mathrm{y}} \end{pmatrix}_{z_p^-} = \mathcal{A}\left(\mathcal{C}_{p-1}^{12} + \mathcal{C}_{p-1}^{34}\mathcal{R}_{p-1}\right) \begin{pmatrix} \mathcal{E}_{p-1\mathrm{x}}^{(1)} \\ \mathcal{E}_{p-1\mathrm{y}}^{(2)} \end{pmatrix} \\ \begin{pmatrix} \mathcal{H}_{p\mathrm{x}} \\ \mathcal{H}_{p\mathrm{y}} \end{pmatrix}_{z_p^-} = \mathcal{B}_{p-1}^{12}\left(\mathcal{C}_{p-1}^{12} - \mathcal{C}_{p-1}^{34}\mathcal{R}_{p-1}\right) \begin{pmatrix} \mathcal{E}_{p-1\mathrm{x}}^{(1)} \\ \mathcal{E}_{p-1\mathrm{y}}^{(2)} \end{pmatrix} \end{cases} , \tag{29}$$

where

$$\mathcal{C}_{p-1}^{k,k+1} \equiv \begin{pmatrix} e^{-i\tilde{\varphi}_{p-1}^{(k)}} & 0 \\ 0 & e^{-i\tilde{\varphi}_{p-1}^{(k+1)}} \end{pmatrix} \qquad k = 1, 3 , \tag{30}$$

with

$$\tilde{\varphi}_{p-1}^{(k)} \equiv q_0 \tilde{n}_{p-1\mathrm{z}}^{(k)} d_{p-1} \ , \qquad k = 1, \ldots, 4 \ .$$

In here $d_p \equiv z_{p+1} - z_p$ is the thickness of layer p, $\tilde{n}_{p-1\mathrm{z}}^{(k)}$ is defined in Eqs. (24) and (25) and q_0 is the propagation constant in vacuum, see Sect. IV B.

Based on Eqs. (27) and (29), the continuity of the tangential components of the electric and magnetic field on the boundary z_p implies that

$$\begin{cases} (\mathcal{I} + \mathcal{R}_p) \begin{pmatrix} \mathcal{E}_{p\mathrm{x}}^{(1)} \\ \mathcal{E}_{p\mathrm{y}}^{(2)} \end{pmatrix} = \left(\mathcal{C}_{p-1}^{12} + \mathcal{C}_{p-1}^{34} \mathcal{R}_{p-1}\right) \begin{pmatrix} \mathcal{E}_{p-1\mathrm{x}}^{(1)} \\ \mathcal{E}_{p-1\mathrm{y}}^{(2)} \end{pmatrix} \\ \mathcal{B}_p^{12} (\mathcal{I} - \mathcal{R}_p) \begin{pmatrix} \mathcal{E}_{p\mathrm{x}}^{(1)} \\ \mathcal{E}_{p\mathrm{y}}^{(2)} \end{pmatrix} = \mathcal{B}_{p-1}^{12} \left(\mathcal{C}_{p-1}^{12} - \mathcal{C}_{p-1}^{34} \mathcal{R}_{p-1}\right) \begin{pmatrix} \mathcal{E}_{p-1\mathrm{x}}^{(1)} \\ \mathcal{E}_{p-1\mathrm{y}}^{(2)} \end{pmatrix} \end{cases} ,$$

such that by eliminating the electric field vectors, one immediately gets

$$\mathcal{D}_{p-1} (1 + \mathcal{R}_p) = \mathcal{B}_p^{12} (\mathcal{I} - \mathcal{R}_p) \ ,$$

where

$$\mathcal{D}_{p-1} \equiv \mathcal{B}_{p-1}^{12} \left(\mathcal{C}_{p-1}^{12} - \mathcal{C}_{p-1}^{34} \mathcal{R}_{p-1}\right) \left(\mathcal{C}_{p-1}^{12} + \mathcal{C}_{p-1}^{34} \mathcal{R}_{p-1}\right)^{-1} \ . \tag{31}$$

$\mathcal{R}_p$ is therefore given in terms of $\mathcal{R}_{p-1}$ by the following simple recursion relation:

$$\mathcal{R}_p = \left(\mathcal{B}_p^{12} + \mathcal{D}_{p-1}\right)^{-1} \left(\mathcal{B}_p^{12} - \mathcal{D}_{p-1}\right) \qquad p = 1, \ldots, N \ . \tag{32}$$

In order to determine the reflectivity matrix $\mathcal{R}_N$ of the surface layer, one has to evaluate all reflectivity matrices $\mathcal{R}_p$ for all layers below the surface layer. This requires to start the iterative procedure at the first layer ($p = 1$) on top of the substrate. But in order to calculate $\mathcal{R}_1$, one needs to know the 2×2 matrix $\mathcal{D}_0$ corresponding to the substrate, see Eq. (32). This in turn, according to Eq. (31) is only the case, if the reflectivity matrix $\mathcal{R}_0$ of the substrate is available. In order to achieve this, one has to formulate the tangential components of the electric and magnetic field at z_1^- by taking into account that the substrate is a semi–infinite bulk without any boundaries and hence $\mathcal{R}_0 = 0$. [18,19] Thus $\mathcal{D}_0 = \mathcal{B}_0^{12}$, which according to Eq. (28) requires to specify the permittivity of the substrate.

3. Surface reflectivity matrix

In the vacuum region, since $\tilde{\epsilon}_{\rm xx} = 1$, $\tilde{\epsilon}_{\rm xy} = 0$, one has to deal with the superposition of only two beams, namely that of the incident and reflected electromagnetic waves. These beams are related through the surface reflectivity matrix $R_{\rm surf}$ such that for polar geometry and normal incidence,

$$\begin{pmatrix} \mathcal{E}^{(\rm r)}_{\rm vac,x} \\ \mathcal{E}^{(\rm r)}_{\rm vac,y} \end{pmatrix} = R_{\rm surf} \begin{pmatrix} \mathcal{E}^{(\rm i)}_{\rm vac,x} \\ \mathcal{E}^{(\rm i)}_{\rm vac,y} \end{pmatrix} \equiv \begin{pmatrix} \tilde{r}_{\rm xx} & \tilde{r}_{\rm xy} \\ -\tilde{r}_{\rm xy} & \tilde{r}_{\rm xx} \end{pmatrix} \begin{pmatrix} \mathcal{E}^{(\rm i)}_{\rm vac,x} \\ \mathcal{E}^{(\rm i)}_{\rm vac,y} \end{pmatrix} , \tag{33}$$

see the Appendix. Thus the tangential components of the electric and magnetic field at a point z^+_{N+1}, namely just above the interface between the vacuum and the surface, are given by

$$\begin{cases} \begin{pmatrix} \mathcal{E}_{\rm vac,x} \\ \mathcal{E}_{\rm vac,y} \end{pmatrix}_{z^+_{N+1}} = (\mathcal{I} + R_{\rm surf}) \begin{pmatrix} \mathcal{E}^{(\rm i)}_{\rm vac,x} \\ \mathcal{E}^{(\rm i)}_{\rm vac,y} \end{pmatrix} \\ \begin{pmatrix} \mathcal{H}_{\rm vac,x} \\ \mathcal{H}_{\rm vac,y} \end{pmatrix}_{z^+_{N+1}} = (B^{12}_{\rm vac} + B^{34}_{\rm vac} R_{\rm surf}) \begin{pmatrix} \mathcal{E}^{(\rm i)}_{\rm vac,x} \\ \mathcal{E}^{(\rm i)}_{\rm vac,y} \end{pmatrix} \end{cases} , \tag{34}$$

where

$$B^{12}_{\rm vac} = \begin{pmatrix} 0 & 1 \\ -1 & 0 \end{pmatrix} \quad \text{and} \quad B^{34}_{\rm vac} = \begin{pmatrix} 0 & -1 \\ 1 & 0 \end{pmatrix} . \tag{35}$$

According to Eqs. (29) and (34), the continuity of the tangential components of the electric and magnetic fields at the vacuum and surface layer interface, $z_{N+1} = 0$, can be written as

$$\begin{cases} (\mathcal{I} + R_{\rm surf}) \begin{pmatrix} \mathcal{E}^{(\rm i)}_{\rm vac,x} \\ \mathcal{E}^{(\rm i)}_{\rm vac,y} \end{pmatrix} = \mathcal{A} (\mathcal{C}^{12}_N + \mathcal{C}^{34}_N \mathcal{R}_N) \begin{pmatrix} \mathcal{E}^{(1)}_{N\rm x} \\ \mathcal{E}^{(2)}_{N\rm y} \end{pmatrix} \\ (B^{12}_{\rm vac} + B^{34}_{\rm vac} R_{\rm surf}) \begin{pmatrix} \mathcal{E}^{(\rm i)}_{\rm vac,x} \\ \mathcal{E}^{(\rm i)}_{\rm vac,y} \end{pmatrix} = \mathcal{B}^{12}_N (\mathcal{C}^{12}_N - \mathcal{C}^{34}_N \mathcal{R}_N) \begin{pmatrix} \mathcal{E}^{(1)}_{N\rm x} \\ \mathcal{E}^{(2)}_{N\rm y} \end{pmatrix} \end{cases} .$$

By eliminating from this system of equations the electric field vectors, it follows that

$$\mathcal{F}_N (1 + R_{\rm surf}) = B^{12}_{\rm vac} + B^{34}_{\rm vac} R_{\rm surf} ,$$

where

$$\mathcal{F}_N \equiv \mathcal{B}^{12}_N \left(\mathcal{C}^{12}_N - \mathcal{C}^{34}_N \mathcal{R}_N\right) \left(\mathcal{C}^{12}_N + \mathcal{C}^{34}_N \mathcal{R}_N\right)^{-1} \mathcal{A}^{-1} = \mathcal{D}_N \mathcal{A}^{-1} . \tag{36}$$

Thus for the surface reflectivity matrix one obtains

$$R_{\rm surf} = \left(\mathcal{F}_N - B^{34}_{\rm vac}\right)^{-1} \left(B^{12}_{\rm vac} - \mathcal{F}_N\right) \ . \tag{37}$$

The surface reflectivity matrix $R_{\rm surf}$ is therefore of the form given in Eq. (33), see also Appendix. In spherical coordinates, one immediately obtains the complex reflectivity of the right– and left–handed circularly polarized light as

$$\tilde{r}_{\pm} = \tilde{r}_{\rm xx} \mp i\tilde{r}_{\rm xy} \ ,$$

which in turn determines the Kerr rotation angle $\theta_{\rm K}$ and ellipticity $\epsilon_{\rm K}$, see Eqs. (9) and (10).

4. Self–consistent layer–resolved permittivities

In order to calculate for a homogeneous, anisotropic layer p the corresponding dielectric tensor (23) from the inter– and intra–layer permittivities defined in Eq. (19), the following linear system of equations

$$\begin{pmatrix} \tilde{\epsilon}^p_{\rm xx} & \tilde{\epsilon}^p_{\rm xy} \\ -\tilde{\epsilon}^p_{\rm xy} & \tilde{\epsilon}^p_{\rm xx} \end{pmatrix} \begin{pmatrix} \mathcal{E}_{p\rm x} \\ \mathcal{E}_{p\rm y} \end{pmatrix} = \sum_{q=1}^{N} \begin{pmatrix} \tilde{\epsilon}^{pq}_{\rm xx} & \tilde{\epsilon}^{pq}_{\rm xy} \\ -\tilde{\epsilon}^{pq}_{\rm xy} & \tilde{\epsilon}^{pq}_{\rm xx} \end{pmatrix} \begin{pmatrix} \mathcal{E}_{q\rm x} \\ \mathcal{E}_{q\rm y} \end{pmatrix}$$

has to be solved, see Eq. (18). Here for $\vec{\mathcal{E}}_p$ one can take the following Ansatz:

$$\begin{pmatrix} \mathcal{E}_{p\rm x} \\ \mathcal{E}_{p\rm y} \end{pmatrix} \equiv \begin{pmatrix} \mathcal{E}_{p\rm x} \\ \mathcal{E}_{p\rm y} \end{pmatrix}_{z=z_p^+ + \frac{d_p}{2}} = \mathcal{A} \left[\left(\mathcal{C}^{12}_p\right)^{\frac{1}{2}} + \left(\mathcal{C}^{34}_p\right)^{\frac{1}{2}} \mathcal{R}_p \right] \begin{pmatrix} \mathcal{E}^{(1)}_{p\rm x} \\ \mathcal{E}^{(2)}_{p\rm y} \end{pmatrix} \ ,$$

where due to Eq. (30),

$$\left(\mathcal{C}^{k,k+1}_p\right)^{\frac{1}{2}} \equiv \begin{pmatrix} e^{-iq_0\tilde{n}^{(k)}_{pz}\frac{d_p}{2}} & 0 \\ 0 & e^{-iq_0\tilde{n}^{(k+1)}_{pz}\frac{d_p}{2}} \end{pmatrix} \qquad k = 1, 3 \ .$$

By using the continuity equation of the tangential components of the electric field at the boundaries, see Eqs. (27), (29) and (34), one then obtains the layer–resolved permittivities as a weighted sum of the inter– and intra–layer permittivities defined in Eq. (19):

$$\begin{pmatrix} \tilde{\epsilon}^p_{\rm xx} & \tilde{\epsilon}^p_{\rm xy} \\ -\tilde{\epsilon}^p_{\rm xy} & \tilde{\epsilon}^p_{\rm xx} \end{pmatrix} = \sum_{q=1}^{N} W_{pq}\, \tilde{\boldsymbol{\epsilon}}^{\,pq} \ . \tag{38}$$

where

$$W_{pq} = \mathcal{A} \left(\prod_{k=0}^{N-q} \mathcal{W}_{q+k} \right) \left(\prod_{k=0}^{N-p} \mathcal{W}_{p+k} \right)^{-1} \mathcal{A}^{-1} \ , \tag{39}$$

with

$$\mathcal{W}_{p+k} = \left(\mathcal{I} + \mathcal{R}_{p+k} \right) \left(\mathcal{C}^{12}_{p+k} + \mathcal{C}^{34}_{p+k} \mathcal{R}_{p+k} \right)^{-1} \ , \qquad k = 1, \ldots, N-p \ ,$$

and

$$\mathcal{W}_{p} = \left[\left(\mathcal{C}^{12}_{p} \right)^{\frac{1}{2}} + \left(\mathcal{C}^{34}_{p} \right)^{\frac{1}{2}} \mathcal{R}_{p} \right] \left(\mathcal{C}^{12}_{p} + \mathcal{C}^{34}_{p} \mathcal{R}_{p} \right)^{-1} \ , \qquad k = 0.$$

Because the 2×2 matrices $\mathcal{W}_{p+k}$ contain $\mathcal{R}_p$, $\mathcal{C}^{12}_p$ and $\mathcal{C}^{34}_p$, which in turn depend on layer–resolved permittivities $\tilde{\epsilon}^{p}_{\mu\nu}(\omega)$, Eq. (38) has to be solved iteratively.

The self–consistent procedure can be started by putting all 2×2 weighting matrices W_{pq} in Eq. (39) to unity, i.e., by neglecting the phase differences of the electromagnetic waves between the lower and upper boundaries in each layer p,

$$\tilde{\epsilon}^{p}_{\mu\nu}(\omega)^{(0)} = \sum_{q=1}^{N} \tilde{\epsilon}^{pq}_{\mu\nu}(\omega) \ . \tag{40}$$

These quantities $\tilde{\epsilon}^{p}_{\mu\nu}(\omega)^{(0)}$ can be used to calculate $\mathcal{R}^{(0)}_p$ in terms of Eqs. (31) and (32). Improved layer–resolved permittivities follow then from Eq. (38). This iterative procedure has to be repeated until the difference in the old and new layer–resolved permittivity of layer p is below a numerical threshold ϵ_p,

$$\max \ \left| \tilde{\epsilon}^{p}_{\mu\nu}(\omega)^{(i+1)} - \tilde{\epsilon}^{p}_{\mu\nu}(\omega)^{(i)} \right| \leq \varepsilon_p \ . \tag{41}$$

V. RESULTS AND DISCUSSIONS

¿From experiments is known that Pt substrates prefer an fcc(111) orientation. [42] Therefore in the present contribution, the calculations for the layered systems Co|Pt_5|Pt(111) and Pt_3|Co|Pt_5|Pt(111) have been performed, with five Pt layers serving as buffer [43] to bulk fcc Pt.

The Fermi level in Eqs. (3) and (4) is that of paramagnetic fcc Pt bulk (lattice parameter of 7.4137 a.u.), which also serves as parent lattice, [43] i.e., no layer relaxation is considered.

A. Paramagnetic fcc(111) Pt substrate

As mentioned above in order to determine the surface reflectivity the permittivity tensor of the semi–infinite substrate has to be evaluated. As can be seen from Fig. 2, the xx–element of the permittivity tensor of the fcc(111) Pt substrate shows a rather simple photon energy dependence. The real part of the permittivity $\tilde{\epsilon}_{\rm xx}(\omega)$ has a peak around 1 eV, while the imaginary part of $\tilde{\epsilon}_{\rm xx}(\omega)$ exhibits an almost perfect hyperbolic frequency dependence. The strong decay of $\tilde{\epsilon}_{\rm xx}(\omega)$ for photon energies in the vicinity of the static limit ($\omega = 0$) can be easily understood in terms of the Eqs. (19) and (40), see also Ref. [13] : for $\omega \to 0$ the real part of $\tilde{\epsilon}_{\rm xx}(\omega)$ must tend to minus infinity whereas the imaginary part has to decrease.

The xy–element of the permittivity tensor for fcc–Pt(111) is identical zero over the whole range of optical frequencies, a functional behavior that of course does not need to be illustrated.

B. Self–consistent layer–resolved permittivities

In terms of the substrate and the zeroth order layer–resolved permittivities, see Eq. (40), the iterative determination of the surface reflectivity matrix described above, provides also self–consistent, layer–resolved permittivities $\tilde{\epsilon}^{p}_{\rm xx}(\omega)$ in a very efficient manner: in less than five iterations an accuracy of $\varepsilon_p = 10^{-13}$ for each layer p, see Eq. (41), can be achieved.

In order to illustrate this procedure, in Fig. 3 the imaginary part of the relative difference between the self–consistent and zeroth order layer–resolved xx–element of the permittivity tensor for Co|Pt_5|Pt(111) with and without Pt cap layers is displayed.

This relative difference is to be viewed as the relative error made by using according to Eq. (40) the 2×2 matrix technique with zeroth order layer–resolved permittivities. As can be seen from Fig. 3, this relative error is layer, frequency and system dependent. The higher the photon energy and the bigger the layered system the less exact are the zeroth order layer–resolved permittivities. However, for relatively small layered systems, the relative error made by using only zeroth order permittivities is typically below 5 % for $\tilde{\epsilon}_{\rm xx}(\omega)$ and less than 20 % for $\tilde{\epsilon}_{\rm xy}(\omega)$. However, the resulting relative error in the Kerr rotation angle and the ellipticity as calculated by comparing the spectra corresponding to the self–consistent and to the zeroth order

layer–resolved permittivities, is always less than 1 %. Therefore, Eq. (40) can be considered as reasonably good approximation for layer–resolved permittivities.

C. Polar Kerr effect for normal incidence

The systems investigated in here refer to a Co mono–layer on the top of a fcc–Pt(111) substrate, considering also the case of three Pt cap layers. As already mentioned, five Pt layers serve as buffer to the semi–infinite host in order to ensure that the induced magnetic moments decrease monotonously to zero into the paramagnetic Pt substrate.

The ab–initio Kerr spectra obtained from self–consistent layer–resolved permittivities by applying the 2×2 matrix technique are shown in Fig. 4. Usually, in experiments Pt cap layers are deposited on top of Co in order to prevent the oxidation of the surface. [44] By performing a separate, magnetic anisotropy calculation, [43] we have found that Co|Pt(111) exhibits perpendicular magnetization only in the presence of Pt cap layers. Therefore, for the polar Kerr spectra of the Co|Pt_5|Pt(111) system shown in Fig. 4 the polar geometry, namely the perpendicular orientation of the magnetization is imposed.

Analyzing in Fig. 4 the Kerr spectra of the capped and that of the uncapped systems, several differences can be observed. The negative peak in the Kerr rotation angle θ_{K} at 3 eV in the spectrum of Co|Pt_5|Pt(111) almost disappears from the spectrum in the case of the capped layered system. In the Kerr ellipticity the zero location at 2.8 eV observed for the uncapped system is shifted to 2.5 eV for the capped system system and simultaneously the infrared (IR) positive peak is shrunk and moved towards lower photon energies. Besides these features, the sign of the ultraviolet (UV) peak in both, the Kerr rotation and ellipticity spectra is changed, when the Co surface layer is capped. This particular feature can also be observed in the Kerr spectra obtained by using the two–media approach, see Fig. 5. In the two–media Kerr rotation spectrum, the negative IR peak at 2 eV in Co|Pt_5|Pt(111) is shifted to about 1 eV in case of the capped system.

Comparing the spectra in Fig. 4 with those in Fig. 5, it is evident that the theoretical Kerr spectra depend indeed on the macroscopic model used to describe the propagation of electromagnetic waves in the system. Because the systems investigated in here are much smaller

than those used in experiments, [44,45] a strict quantitative comparison with experimental data cannot be made. However, a qualitative comparison based on the well–known, general features of the Co|Pt experimental Kerr spectra is still possible: [45] the Kerr rotation angle shows (a) a small negative IR peak at 1.5 eV, which decreases in amplitude with decreasing Co thickness, and (b) a high and broad negative UV peak, which moves from 4.1 eV to 3.9 eV for increasing Co thickness. The Kerr ellipticity is characterized by (a) a shift of the zero location at 1.5 eV (pure Co film) to 3.7 eV with decreasing Co thickness, (b) a positive peak around 3 eV and (c) a shift of the minimum at 4.9 eV in pure Co film towards higher photon energies.

In the Kerr rotation spectra of the capped system shown in Fig. 4, there is no negative IR peak around 1.5 eV, but a negative UV exists at 5.5 eV. The Kerr ellipticity spectra of the capped system in Fig. 4, has a zero location at 2.5 eV and positive peaks show up at 0.5, 3.5, 4 and 5 eV. These features suggest that in the case of $Pt_3\,|Co|Pt_5\,|Pt(111)$ the Kerr spectra obtained by applying the 2×2 matrix technique are typical for Co|Pt layered systems.

A similar investigation of the Kerr rotation spectra in Fig. 5, reveals that for the capped system there are two negative IR peaks at 1, 1.5 eV and a negative UV peak around 5 eV. The Kerr ellipticity for the capped system in Fig. 5 shows a zero location at 1 eV (1.5 eV in case of a pure Co film), two positive peaks at 4 and 5 eV and a small negative peak around 3 eV. All these features make the Kerr spectra of $Pt_3\,|Co|Pt_5\,|Pt(111)$ described via the two–media approach to resemble those of a pure Co film rather than those of a Co|Pt layered system.

Previous results obtained by applying the 2×2 matrix technique using as substrate permittivity that of the last Pt–layer below the Co one, [46] have shown similar characteristics in the Kerr spectra. Hence, these features cannot be ascribed to the presence of the substrate. In an other contribution, [31] it was shown that the optical conductivity of these systems is dominated by the contributions arising from the polarized Pt–layers. Therefore, the pure Co film–like spectra obtained for $Pt_3\,|Co|Pt_5\,|Pt(111)$ within the two–media approach can be seen as an indication that a layered system cannot be approximated by a homogeneous medium in which no optical reflections or interferences occur.

VI. SUMMARY

We have used the 2×2 matrix technique for the most frequently used experimental set–up, namely for polar geometry and normal incidence. This technique allows one to account for all multiple reflections and optical interferences in a semi–infinite layered system. The Kerr rotation angle and ellipticity can be directly obtained from the iteratively calculated surface reflectivity matrix, which in turn can be used to determine layer–resolved permittivities self–consistently. For free surface of layered systems realistic ab–initio Kerr spectra are obtained using the inter– and intra–layer conductivities as given by Luttinger's formula within the spin–polarized relativistic screened Korringa–Kohn–Rostoker method.

A comparison of the theoretical Kerr spectra of Co|Pt_5|Pt(111) and Pt_3 |Co|Pt_5|Pt(111) as obtained by applying the 2×2 matrix technique and the two–media approach indicates that the former technique provides typical results for layered systems, whereas the later approach tends to generate spectra specific for homogeneous films on top of a substrate.

ACKNOWLEDGMENTS

This work was supported by the Austrian Ministry of Science (Contract No. 45.451), by the Hungarian National Science Foundation (Contract No. OTKA T030240 and T029813) and partially by the RTN network "Computational Magnetoelectronics" (Contract No. HPRN–CT–2000-00143).

APPENDIX: SYMMETRY OF REFLECTIVITY MATRICES

Since for a semi–infinite substrate, $\mathcal{R}_0 = 0$, $\mathcal{D}_0 = \mathcal{B}_0^{12}$, with $\mathcal{B}_0^{12}$ as given by Eq. (28), according to Eq. (32), the reflectivity matrix of the first layer on top of the substrate is given by

$$\mathcal{R}_1 = \begin{pmatrix} \tilde{r}_1 & 0 \\ 0 & \tilde{r}_1' \end{pmatrix} ,$$

where

$$\begin{cases} \tilde{r}_1 \;=\; \dfrac{\tilde{n}^{(1)}_{1z} - \tilde{n}^{(1)}_{0z}}{\tilde{n}^{(1)}_{1z} + \tilde{n}^{(1)}_{0z}} \\ \\ \tilde{r}'_1 \;=\; \dfrac{\tilde{n}^{(2)}_{1z} - \tilde{n}^{(2)}_{0z}}{\tilde{n}^{(2)}_{1z} + \tilde{n}^{(2)}_{0z}} \end{cases} \quad .$$

Assuming that all $p-1$ reflectivity matrices are of this diagonal form, namely

$$\mathcal{R}_j = \begin{pmatrix} \tilde{r}_j & 0 \\ 0 & \tilde{r}'_j \end{pmatrix}, \qquad j = 1, \ldots, (p-1) \;\; ,$$

by taking into account Eqs. (28) and (30), Eq. (31) immediately yields

$$\mathcal{D}_{p-1} = \begin{pmatrix} -i\tilde{d}_{p-1} & -\tilde{d}'_{p-1} \\ \tilde{d}_{p-1} & i\tilde{d}'_{p-1} \end{pmatrix} \;\; ,$$

where

$$\begin{cases} \tilde{d}_{p-1} \;=\; \tilde{n}^{(1)}_{p-1z} \dfrac{e^{-i\tilde{\varphi}^{(1)}_{p-1}} - e^{-i\tilde{\varphi}^{(3)}_{p-1}} \tilde{r}_{p-1}}{e^{-i\tilde{\varphi}^{(1)}_{p-1}} + e^{-i\tilde{\varphi}^{(3)}_{p-1}} \tilde{r}_{p-1}} \\ \\ \tilde{d}'_{p-1} \;=\; \tilde{n}^{(2)}_{p-1z} \dfrac{e^{-i\tilde{\varphi}^{(2)}_{p-1}} - e^{-i\tilde{\varphi}^{(4)}_{p-1}} \tilde{r}'_{p-1}}{e^{-i\tilde{\varphi}^{(2)}_{p-1}} + e^{-i\tilde{\varphi}^{(4)}_{p-1}} \tilde{r}'_{p-1}} \end{cases} \quad .$$

The reflectivity matrix of layer p as obtained from the recursion relation (32) is found to be also diagonal

$$\mathcal{R}_p = \begin{pmatrix} \tilde{r}_p & 0 \\ 0 & \tilde{r}'_p \end{pmatrix} \;\; ,$$

where

$$\begin{cases} \tilde{r}_p \;=\; \dfrac{\tilde{n}^{(1)}_{pz} - \tilde{d}_{p-1}}{\tilde{n}^{(1)}_{pz} + \tilde{d}_{p-1}} \\ \\ \tilde{r}'_p \;=\; \dfrac{\tilde{n}^{(2)}_{pz} - \tilde{d}'_{p-1}}{\tilde{n}^{(2)}_{pz} - \tilde{d}'_{p-1}} \end{cases} \;\; ,$$

i.e., all the layer–resolved reflectivity matrices $\mathcal{R}_j$ ($j = 1, \ldots, N$) are diagonal matrices as was anticipated in Eq. (26).

In terms of the diagonal reflectivity matrix of the surface layer $\mathcal{R}_N$, and $\mathcal{A}$ and $\mathcal{B}^{12}_N$ as given by Eq. (28), Eq. (36) reduces to

$$\mathcal{F}_N = \frac{1}{2} \begin{pmatrix} i\tilde{f}_N & -\tilde{f}'_N \\ \tilde{f}'_N & i\tilde{f}_N \end{pmatrix} \;\; ,$$

where

$$\begin{cases} \tilde{f}_N &= \tilde{d}'_N - \tilde{d}_N \\ \tilde{f}'_N &= \tilde{d}'_N + \tilde{d}_N \end{cases} .$$

By using $\mathcal{F}_N$ together with the matrices defined in Eq. (35) in Eq. (37), the resulting surface reflectivity matrix is of the form anticipated in Eq. (33), i.e.

$$R_{\text{surf}} = \begin{pmatrix} \tilde{r}_{\text{xx}} & \tilde{r}_{\text{xy}} \\ -\tilde{r}_{\text{xy}} & \tilde{r}_{\text{xx}} \end{pmatrix} ,$$

where

$$\begin{cases} \tilde{r}_{\text{xx}} &= \dfrac{-\tilde{f}_N^2 + \tilde{f}_N'^2 - 4}{\tilde{f}_N^2 - \tilde{f}_N'^2 + 4\left(\tilde{f}'_N - 1\right)} \\ \tilde{r}_{\text{xy}} &= -4i\dfrac{\tilde{f}_N}{\tilde{f}_N^2 - \tilde{f}_N'^2 + 4\left(\tilde{f}'_N - 1\right)} \end{cases} .$$

REFERENCES

[1] W. R. Bennett, W. Schwarzacher, and W. F. Egelhoff, Phys. Rev. Letters **65**, 3169 (1990).

[2] T. K. Hatwar, Y. S. Tyan, and C. F. Brucker, J. Appl. Physics **81**, 3839 (1997).

[3] Y. Suzuki, T. Katayama, P. B. S. Yuasa, and E. Tamura, Phys. Rev. Letters **80**, 5200 (1998).

[4] G. A. Bertero and R. Sinclair, J. Magn. Magn. Materials **134**, 173 (1994).

[5] P. M. Oppeneer, T. Maurer, J. Sticht, and J. Kübler, Phys. Rev. B **45**, 10924 (1992).

[6] L. Szunyogh, B. Újfalussy, P. Weinberger, and J. Kollár, Phys. Rev. B **49**, 2721 (1994).

[7] L. Szunyogh, B. Újfalussy, and P. Weinberger, Phys. Rev. B **51**, 9552 (1995).

[8] B. Újfalussy, L. Szunyogh, and P. Weinberger, Phys. Rev. B **51**, 12836 (1995).

[9] J. Callaway, *Quantum Theory of the Solid State part B* (Academic Press, New York, 1974).

[10] P. M. Oppeneer, Theory of the magneto–optical Kerr effect in ferromagnetic compounds, Habilitationsschrift, Technische Universität Dresden, 1999.

[11] L. Szunyogh and P. Weinberger, J. Phys.: Condensed Matter **11**, 10451 (1999).

[12] J. M. Luttinger, in *Mathematical Methods in Solid State and Superfluid Theory*, edited by R. C. Clark and G. H. Derrick (Oliver and Boyd, Edingburgh, 1967), Chap. 4: Transport theory, p. 157.

[13] A. Vernes, L. Szunyogh, and P. Weinberger, Phase Transitions in press (2001).

[14] W. Reim and J. Schoenes, in *Magneto–optical spectroscopy of f–electron systems*, ferromagnetic materials ed., edited by K. H. J. Buschow and E. P. Wohlfarth (North–Holland, Amsterdam, 1990), Vol. 5, Chap. 2, p. 133.

[15] F. Abelés, Ann. Phys. (France) **5**, 596 (1950).

[16] D. O. Smith, Opt. Acta **12**, 13 (1965).

[17] R. P. Hunt, J. Appl. Physics **38**, 1652 (1967).

[18] M. Mansuripur, J. Appl. Physics **67**, 6466 (1990).

[19] M. Mansuripur, *The principles of Magneto-Optical Recording* (Cambridge University Press, Cambridge, 1995).

[20] P. Yeh, Surf. Sci. **96**, 41 (1980).

[21] J. Zak, E. R. Moog, C. Liu, and S. D. Bader, J. Magn. Magn. Materials **89**, 107 (1990).

[22] R. Atkinson and P. H. Lissberger, J. Magn. Magn. Materials **118**, 271 (1993).

[23] R. Kubo, J. Phys. Soc. Japan **12**, 570 (1957).

[24] B. Y.-K. Hu, Am. J. Phys. **61**, 457 (1993).

[25] G. D. Mahan, *Many–Particle Physics* (Plenum Press, New York, 1990).

[26] M. Lax, Phys. Rev. **109**, 1921 (1958).

[27] D. M. C. Nicholson *et al.*, Phys. Rev. B **50**, 14 686 (1994).

[28] K. Wildberger, P. Lang, R. Zeller, and P. H. Dederichs, Phys. Rev. B **52**, 11 502 (1995).

[29] W. H. Butler, Phys. Rev. B **31**, 3260 (1985).

[30] P. Weinberger *et al.*, J. Phys.: Condensed Matter **8**, 7677 (1996).

[31] A. Vernes, L. Szunyogh, and P. Weinberger, J. Magn. Magn. Materials in press (2001).

[32] A. Vernes, L. Szunyogh, and P. Weinberger, J. Phys.: Condensed Matter **13**, 1529 (2001).

[33] D. P. Laurie, Math. Comput. **66**, 1133 (1997).

[34] D. Calvetti, G. H. Golub, W. B. Gragg, and L. Reichel, Math. Comput. **69**, 1035 (2000).

[35] W. H. Press, B. P. Flannery, S. A. Teukolsky, and W. T. Vetterling, *Numerical recipes in Fortran: The art of scientific computing* (Cambridge University Press, Cambridge, 1992).

[36] J. Hama and M. Watanabe, J. Phys.: Condensed Matter **4**, 4583 (1992).

[37] N. W. Ashcroft and N. D. Mermin, *Solid State Physics* (Saunders College Publishing, Fort Worth, 1976).

[38] V. M. Agranovich and V. L. Ginzburg, in *Spatial dispersion in crystal optics and the theory of excitons*, Vol. XVIII of *Interscience monographs and texts in physics and astronomy*, edited by R. E. Marshak (John Wiley & Sons, London, 1966).

[39] W. H. Butler, X. G. Zhang, D. M. C. Nicholson, and J. M. MacLaren, J. Appl. Physics **76**, 6808 (1994).

[40] L. D. Landau and E. M. Lifshitz, *Electrodynamics of continuous media*, Vol. 8 of *Course of Theoretical Physics* (Butterworth–Heinemann, Oxford, 1999).

[41] A. K. Zvezdin and V. A. Kotov, *Modern magnetooptics and magnetooptical materials*, *Studies in condensed matter physics* (Institut of Physics Publishing, Bristol, 1997).

[42] D. Weller *et al.*, Appl. Physics Lett. **61**, 2726 (1992).

[43] U. Pustogowa *et al.*, Phys. Rev. B **60**, 414 (1999).

[44] R. A. Fry, L. H. Bennett, and E. D. Torre, J. Appl. Physics **87**, 5765 (2000).

[45] S. Uba *et al.*, Phys. Rev. B **53**, 6526 (1996).

[46] A. Vernes, L. Szunyogh, and P. Weinberger, J. Appl. Physics in press (2001).

TABLES

k	1	2	3	4
$\mathcal{E}_{p\mathrm{x}}^{(k)}$	arbitrary	$i\mathcal{E}_{p\mathrm{y}}^{(2)}$	arbitrary	$i\mathcal{E}_{p\mathrm{y}}^{(4)}$
$\mathcal{E}_{p\mathrm{y}}^{(k)}$	$i\mathcal{E}_{p\mathrm{x}}^{(1)}$	arbitrary	$i\mathcal{E}_{p\mathrm{x}}^{(3)}$	arbitrary
$\mathcal{E}_{pz}^{(k)}$	0	0	0	0

TABLE I. Solutions of the Helmholtz equation (21) for polar geometry and normal incidence neglecting the difference in the diagonal elements of the layer–resolved permittivity. $\mathcal{E}_{p\mu}^{(k)}$ is the amplitude of the electric field in layer p for beam k.

k	1	2	3	4
$\mathcal{H}_{p\mathrm{x}}^{(k)}$	$i\mathcal{E}_{p\mathrm{x}}^{(1)}\sqrt{\tilde{\epsilon}_{\mathrm{xx}}^{p}+i\tilde{\epsilon}_{\mathrm{xy}}^{p}}$	$\mathcal{E}_{p\mathrm{y}}^{(2)}\sqrt{\tilde{\epsilon}_{\mathrm{xx}}^{p}-i\tilde{\epsilon}_{\mathrm{xy}}^{p}}$	$-i\mathcal{E}_{p\mathrm{x}}^{(3)}\sqrt{\tilde{\epsilon}_{\mathrm{xx}}^{p}+i\tilde{\epsilon}_{\mathrm{xy}}^{p}}$	$-\mathcal{E}_{p\mathrm{y}}^{(4)}\sqrt{\tilde{\epsilon}_{\mathrm{xx}}^{p}-i\tilde{\epsilon}_{\mathrm{xy}}^{p}}$
$\mathcal{H}_{p\mathrm{y}}^{(k)}$	$-\mathcal{E}_{p\mathrm{x}}^{(1)}\sqrt{\tilde{\epsilon}_{\mathrm{xx}}^{p}+i\tilde{\epsilon}_{\mathrm{xy}}^{p}}$	$-i\mathcal{E}_{p\mathrm{y}}^{(2)}\sqrt{\tilde{\epsilon}_{\mathrm{xx}}^{p}-i\tilde{\epsilon}_{\mathrm{xy}}^{p}}$	$\mathcal{E}_{p\mathrm{x}}^{(3)}\sqrt{\tilde{\epsilon}_{\mathrm{xx}}^{p}+i\tilde{\epsilon}_{\mathrm{xy}}^{p}}$	$i\mathcal{E}_{p\mathrm{y}}^{(4)}\sqrt{\tilde{\epsilon}_{\mathrm{xx}}^{p}-i\tilde{\epsilon}_{\mathrm{xy}}^{p}}$
$\mathcal{H}_{pz}^{(k)}$	0	0	0	0

TABLE II. Solutions of the curl Maxwell equation (22) for polar geometry and normal incidence neglecting the difference in the diagonal elements of the layer–resolved permittivity $\boldsymbol{\epsilon}^{p}$. $\mathcal{H}_{p\mu}^{(k)}$ is the amplitude of the magnetic field in layer p for beam k.

FIGURES

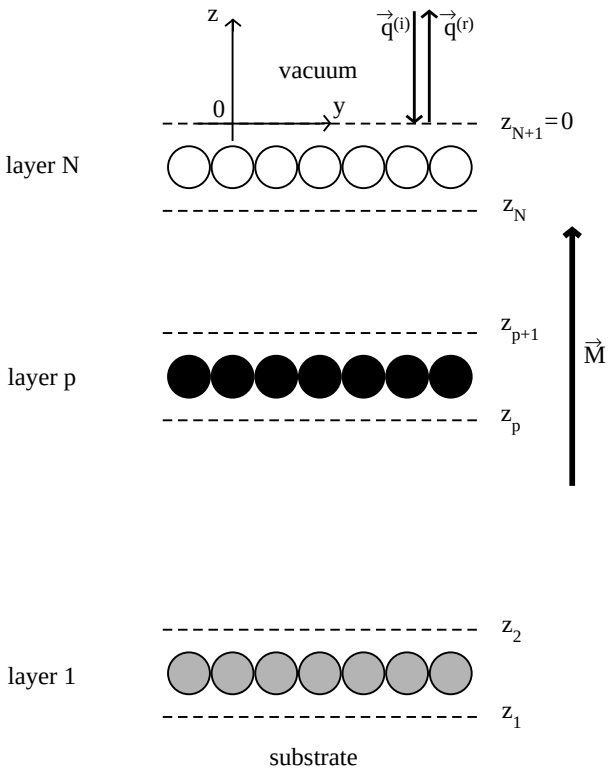

FIG. 1. The macroscopic model used for a layered system within the 2×2 matrix technique for polar geometry and normal incidence. The x axis is perpendicular to the plane of the figure, $\vec{q}^{(i)}$ is the incident and $\vec{q}^{(r)}$ is the reflected wave vector. $\vec{M}$ denotes the total spontaneous magnetization of the system.

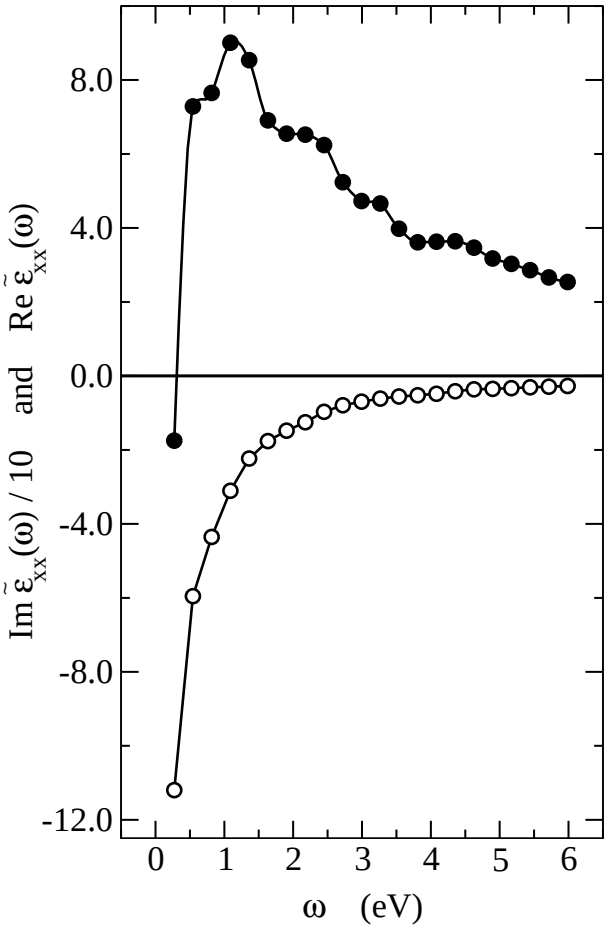

FIG. 2. The permittivity for fcc(111)–Pt bulk as a function of the photon energy ω. The real part of the permittivity is denoted by full circles, the imaginary part by open circles.

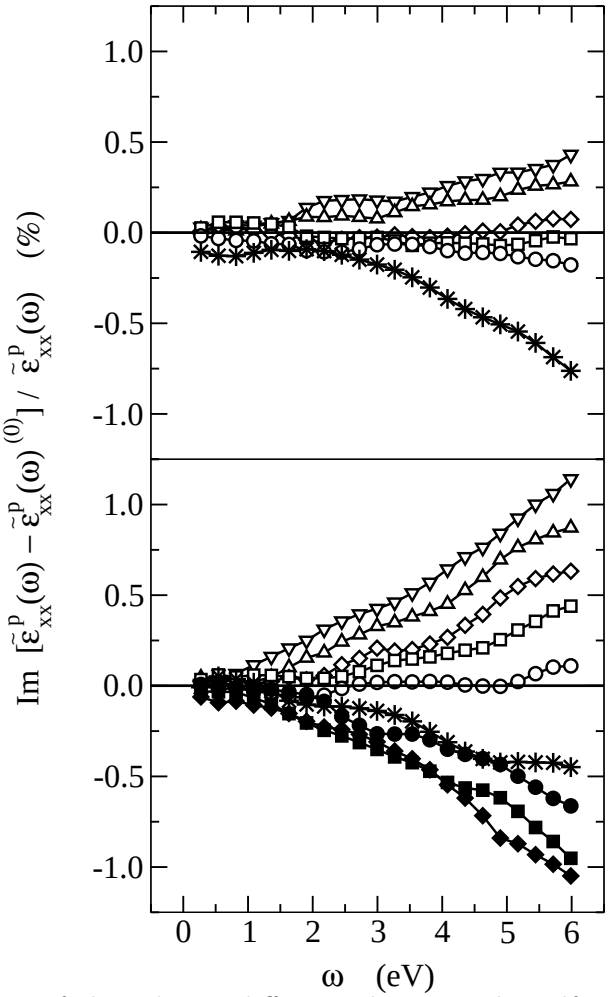

FIG. 3. Imaginary part of the relative difference between the self–consistent and zeroth order layer–resolved xx–element of the permittivity tensor as a function of the photon energy ω for fcc Co|Pt_5|Pt(111) (top) and Pt_3|Co|Pt_5|Pt(111) (bottom). The data represented by full (open) circles correspond to the first, squares to the second and diamonds to the third Pt layer on top of (under) the Co layer (stars). Open triangles down (up) denote the first (second) Pt layer data on top of a paramagnetic fcc–Pt(111) substrate.

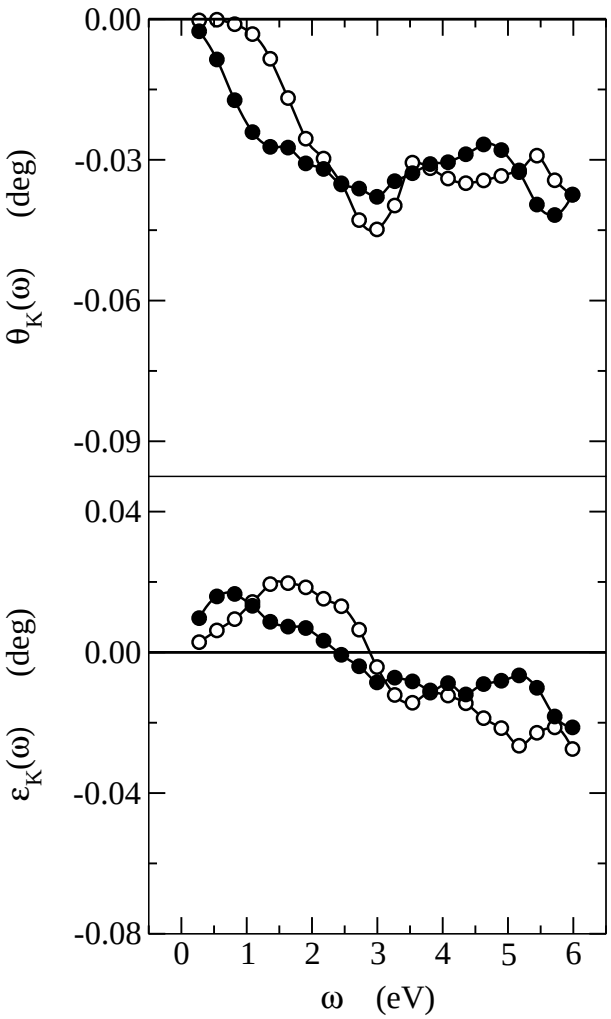

FIG. 4. The magneto–optical Kerr rotation angle $\theta_{\rm K}(\omega)$ and ellipticity $\epsilon_{\rm K}(\omega)$ for polar geometry and normal incidence as a function of the photon energy ω obtained by applying the 2×2 matrix technique for the self–consistent layer–resolved permittivities of fcc Co|Pt_5|Pt(111) (open circles) and Pt_3|Co|Pt_5|Pt(111) (full circles).

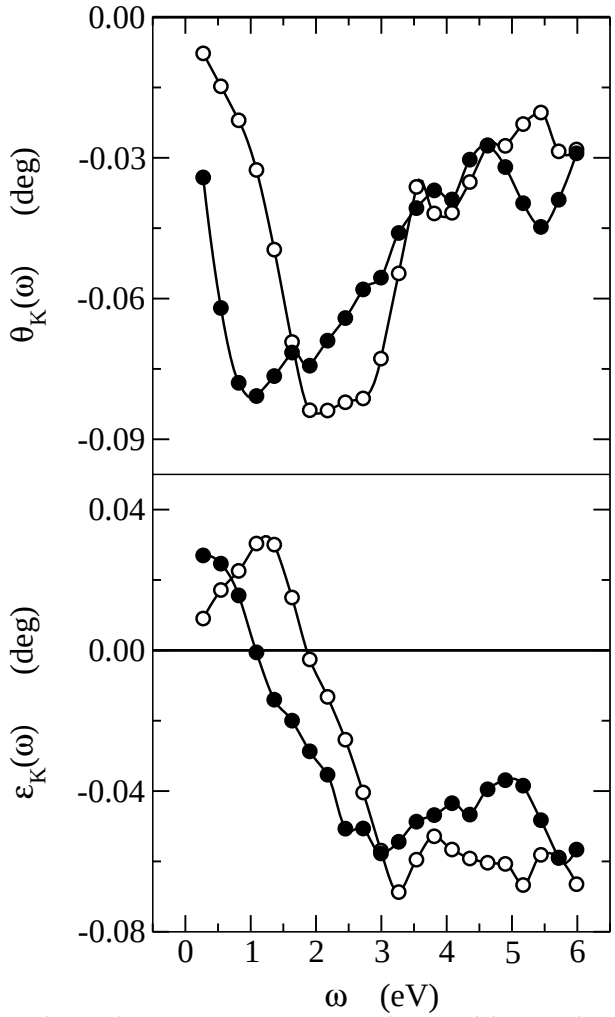

FIG. 5. As in Fig. 4, but here the Kerr spectra was obtained by applying the two–media approach for fcc Co|Pt_5|Pt(111) (open circles) and Pt_3|Co|Pt_5|Pt(111) (full circles).